Journal of Computational Physics 317 (2016) 185–203

Contents lists available at ScienceDirect

Journal of Computational Physics

www.elsevier.com/locate/jcp

An algorithm for prescribed mean curvature using isogeometric methods

Aníbal Chicco-Ruiz, Pedro Morin *, M. Sebastian Pauletti

Instituto de Matemática Aplicada del Litoral, UNL, CONICET, FIQ, Santa Fe, Argentina

ARTICLE INFO

Article history:
Received 12 November 2015
Received in revised form 30 March 2016
Accepted 5 April 2016
Available online 20 April 2016

Keywords:
Minimal surfaces
Prescribed curvature
Isogeometric analysis
Quasi-Newton

ABSTRACT

We present a Newton type algorithm to find parametric surfaces of prescribed mean curvature with a fixed given boundary. In particular, it applies to the problem of minimal surfaces. The algorithm relies on some global regularity of the spaces where it is posed, which is naturally fitted for discretization with isogeometric type of spaces. We introduce a discretization of the continuous algorithm and present a simple implementation using the recently released isogeometric software library `igatools`. Finally, we show several numerical experiments which highlight the convergence properties of the scheme.

1. Introduction

The problem of minimal surfaces is one of the most celebrated in the calculus of variations. The question is to find, among all surfaces with a prescribed boundary (a closed curve), one that is of minimal area. One can realize experimentally such surfaces by dipping a wire into soapy water [1,2]. The mathematics of the problem has been extensively studied, see for example [3,4]. Minimal surfaces are characterized by having zero mean curvature. This last characterization allows us to generalize the problem to that of finding surfaces with a given prescribed (constant) mean curvature. The latter is an important problem appearing in relativity theory as well as in models for hanging drops, soap films and the limiting behavior of phase transition interfaces in the Van der Waals–Cahn–Hilliard theory [5,6].

As minimal surfaces are smooth (provided their boundary is), using spaces of high regularity in the numerical schemes used to compute them should be very suitable. One class of such spaces are the *isogeometric spaces*, which were originally introduced in [7], inspired by the desire to unify the fields of computer aided geometrical design (CAGD) and the finite element method (FEM). The mainly advertised feature of an isogeometric space has been the ability to describe exactly CAGD type geometries. But in addition to exact representation of CAGD geometries the use of B-spline functions allows global smoothness beyond the classical C^0 continuity of standard finite elements: this permits the design of novel numerical schemes that would be extremely difficult to obtain with standard finite elements. For example, we can work with surfaces which have a continuous normal.

The goal of this work is to present a novel fixed point method of Newton type to approximate minimal surfaces and surfaces of prescribed constant mean curvature. We first introduce an idealized version at the continuous level and then discretize it using isogeometric spaces. Finally this discrete scheme is implemented using the isogeometric software library `igatools` [8].

* Corresponding author.
E-mail addresses: achicco@santafe-conicet.gov.ar (A. Chicco-Ruiz), pmorin@santafe-conicet.gov.ar (P. Morin), pauletti@santafe-conicet.gov.ar (M.S. Pauletti).

http://dx.doi.org/10.1016/j.jcp.2016.04.012
0021-9991/

We demonstrate numerically the convergence and stability of the method. The use of high regularity spaces allows us to determine convergence in terms of curvature even when the exact solution is not known.

It is worth recalling that a numerical scheme based on (linear) finite elements was proposed for the Plateau problem in the parametric case by Dziuk and Hutchinson [9]. They transform the Plateau problem into that of finding a parametrization of the unit circle onto the prescribed boundary in such a way that the image of the resulting harmonic extension is a minimal surface. They use the fact that the minimal surface is stationary for the Dirichlet energy among all harmonic maps that span the boundary γ. Other algorithms based on finite differences and C^0 finite elements have been proposed and studied (see [9] and the references therein). Their intricate approach was necessary to circumvent the lack of regularity of the involved spaces, restricted to surfaces that are homeomorphic to a disc. Recently, an algorithm using high-order polynomials has been proposed by Tråsdal and Rønquist [10]. Extensions for the case of prescribed mean curvatures appear in [5,6].

Our approach is very simple, in the sense that we solve the original problem as it is stated without reformulation. This is so as it relies on the fact that the iterates are smooth surfaces. Moreover, our method is not restricted to surfaces that are homeomorphic to a disc, it only requires the boundary to be the one of a given surface.

2. Preliminaries (differential geometry)

In this section we introduce some notation while recalling some concepts from differential geometry necessary to state the minimal surface problem.

2.1. Regular surfaces

For the sake of understanding and to avoid technicalities which do not change the essential content, we will restrict to surfaces that can be parametrized by a single patch. The method applies to more general surfaces (see Section 4.3).

A C^m *regular surface* Γ ($m \geq 1$) is a subset of $\mathbb{R}^3$ such that there exists a continuous map (homeomorphic to its image) $X : \bar{\Omega} \to \mathbb{R}^3$ with Ω an open subset of $\mathbb{R}^2$, satisfying that: $X \in C^m(\Omega; \mathbb{R}^3)$, $\Gamma = X(\Omega)$ and $G(P) := (DX^T DX)(P)$ is invertible for every $P \in \Omega$, where $DX(P)$ is the derivative of X at P (this is called the regularity condition). Let $\mathcal{R}^m(\Omega)$ be the set of all the mappings X that define a C^m regular surface, which from now on will be referred to as parametrizations of that surface. We will refer to C^m regular surfaces simply as regular surfaces, and keep $m \geq 1$ fixed throughout the rest of this article.

At each point p on a regular surface Γ both the *tangent plane* $T_p(\Gamma)$ and the *normal* $\boldsymbol{n}$ are well defined (i.e. independent of the parametrization[1]). In this context Γ is always orientable. In particular $T_p(\Gamma)$ is the image of $\mathbb{R}^2$ by $DX(P)$, and the normal space is the orthogonal complement of $T_p(\Gamma)$.

For a regular surface Γ, its area element measure dp is well defined. Its surface area in terms of a given parametrization $X : \Omega \to \mathbb{R}^2$ is

$$\text{Area}(\Gamma) = J(X) = \int_\Gamma dp = \int_\Omega \sqrt{g}\, dP, \tag{1}$$

where $g = \det G = \det DX^T DX$.

2.2. Surfaces of minimal area

The problem can be stated in a geometrical manner as follows. Let Γ_0 be a regular surface and $\gamma = \partial\Gamma_0$. Let $\mathcal{S}(\gamma) = \{\Gamma \text{ regular surface with } \partial\Gamma = \gamma\}$. The surface of minimal area is a solution Γ^* to the following problem:

$$\Gamma^* = \underset{\Gamma \in \mathcal{S}(\gamma)}{\arg\min}\ \text{Area}(\Gamma). \tag{2}$$

In terms of parametrizations, with a slight abuse of notation, it can be equivalently written as follows. Given $X^0 \in \mathcal{R}^m(\Omega)$, let $\gamma = X^0|_{\partial\Omega}$ and $\mathcal{S}(\gamma) = \{X \in \mathcal{R}^m(\Omega) : X|_{\partial\Omega} = \gamma\}$,

$$\text{Find } X^* \text{ in } \mathcal{S}(\gamma) \text{ such that } \quad X^* = \underset{X \in \mathcal{S}(\gamma)}{\arg\min}\ J(X). \tag{3}$$

To approach problem (3) with the techniques of the calculus of variations we recall some concepts of the calculus on surfaces.

[1] Up to a sign for the normal.

2.3. Calculus on surfaces

Let $\boldsymbol{f}:\Gamma\to\mathbb{R}^3$ be a vector field. We say that $\boldsymbol{f}$ is smooth (C^k) if $\boldsymbol{f}\circ X:\Omega\subset\mathbb{R}^2\to\mathbb{R}^3$ is smooth (C^k) in the sense of Euclidean calculus for any (smooth C^m) parametrization X of Γ ($k\leq m$). In this case the *tangential derivative* of $\boldsymbol{f}$ at p is defined as the linear operator $D_\Gamma\boldsymbol{f}(p):T_p(\Gamma)\to\mathbb{R}^3$, given by

$$D_\Gamma\boldsymbol{f}(p)[\boldsymbol{v}]=\frac{d}{dt}(\boldsymbol{f}\circ\alpha)(t)|_{t=0}, \tag{4}$$

where $\boldsymbol{v}$ is a given element of $T_p(\Gamma)$, and $\alpha:(-\epsilon,\epsilon)\to\Gamma$, any smooth curve on Γ with $\alpha(0)=p$ and $\alpha'(0)=\boldsymbol{v}$. Given a field $\boldsymbol{f}$ on a surface Γ and a parametrization X, we define $\boldsymbol{F}=\boldsymbol{f}\circ X$ the pull-back of $\boldsymbol{f}$. Choosing an orthonormal basis of $\mathbb{R}^3$, the 3×3 matrix

$$(D\boldsymbol{F}G^{-1}DX^T)(P) \tag{5}$$

is the representation of the operator $D_\Gamma\boldsymbol{f}\Pi(p):\mathbb{R}^3\to\mathbb{R}^3$, where $p=X(P)$ and $\Pi(p)=(I-\boldsymbol{n}\otimes\boldsymbol{n})$ is the projection to the tangent plane $T_p(\Gamma)$ with matrix representation

$$(DXG^{-1}DX^T)(P). \tag{6}$$

The surface divergence of the vector field is defined as

$$div_\Gamma\boldsymbol{f}(p)=\sum_{i=1,2}D_\Gamma\boldsymbol{f}(p)[\boldsymbol{e}_i]\cdot\boldsymbol{e}_i \tag{7}$$

with $\{\boldsymbol{e}_1,\boldsymbol{e}_2\}$ any orthonormal basis of $T_p(\Gamma)$.

Remark 2.1 *(Push-forward and pull-back).* Unless stated otherwise in this work we use the following convention. Lowercase letters represent fields defined on a surface Γ and the corresponding uppercase of the letter refers to its pull-back on Ω through a given parametrization X. For example, if u is a field (scalar, vector or tensor-valued) on the surface Γ, we define its pull-back by $U=u\circ X$. Similarly if U is defined on Ω, its push-forward is $u=U\circ X^{-1}$.

2.4. Curvatures

A regular surface has a smooth unit normal vector field $\boldsymbol{n}:\Gamma\to\mathbb{R}^3$. Its tangential derivative $D_\Gamma\boldsymbol{n}(p):T_p(\Gamma)\to\mathbb{R}^3$ encodes the information about the surface curvature. As a matter of fact $D_\Gamma\boldsymbol{n}(p)[T_p(\Gamma)]\subset T_p(\Gamma)$ and when restricted to this tangent plane is a symmetric linear transformation. Indeed, the principal curvatures κ_1 and κ_2 and principal directions are the eigenvalues and the eigenvectors of $D_\Gamma\boldsymbol{n}$. The *mean curvature* H and the *Gaussian curvature* K are

$$H=\kappa_1+\kappa_2=\mathrm{tr}(D_\Gamma\boldsymbol{n}),\qquad K=\kappa_1\kappa_2=\det(D_\Gamma\boldsymbol{n}).$$

Notice also that $D_\Gamma\boldsymbol{n}(p)^T:\mathbb{R}^3\to T_p(\Gamma)$.

3. The problem

In this section we present the problem object of the present work. Two results about the variational derivatives are presented in Lemmas 3.1 and 4.1. The proofs are omitted as they are standard and can be found for example in [3,11,12]. Let Ω be an open and connected set of $\mathbb{R}^2$ and recall the notation from problem (3). There is a given $X^0\in\mathcal{R}^m(\Omega)$, where $\gamma=X^0|_{\partial\Omega}$ is a Jordan curve and $\mathcal{S}(\gamma)=\{X\in\mathcal{R}^m(\Omega):X|_{\partial\Omega}=\gamma\}$.

3.1. The Plateau problem

Finding a surface of minimal area in problem (3) can be very difficult, a simpler associated problem is to find the critical points of J from (1). This is to say find $X\in\mathcal{S}(\gamma)$ such that $J'(X)=0$ which is known as the Plateau problem. Here the prime denotes the variational derivative. To define J' we consider the space of vector increments

$$\boldsymbol{\mathcal{V}}=\{\boldsymbol{V}\in C^m(\Omega;\mathbb{R}^3):\boldsymbol{V}|_{\partial\Omega}=\boldsymbol{0}\},\quad\text{with norm }\|\boldsymbol{V}\|_{\boldsymbol{\mathcal{V}}}=\max_{|\alpha|\leq m}\max_{x\in\Omega}|D^\alpha\boldsymbol{V}(P)|,$$

and let J' be the only bounded linear functional from $\boldsymbol{\mathcal{V}}\to\mathbb{R}$ such that

$$J(X+\boldsymbol{U})=J(X)+J'(X)[\boldsymbol{U}]+o(\|\boldsymbol{U}\|_{\boldsymbol{\mathcal{V}}}),$$

for all $\boldsymbol{U}\in\boldsymbol{\mathcal{V}}$ with $\|\boldsymbol{U}\|_{\boldsymbol{\mathcal{V}}}$ sufficiently small. The following lemma is well known, and proved in the appendix for the sake of completeness.

Lemma 3.1 *(First variation of J). Given $X \in \mathcal{R}^m(\Omega)$ and $\Gamma = X(\Omega)$, if $J(X)$ is the area of Γ, then*

$$J'(X)[\boldsymbol{U}] = \int_\Gamma div_\Gamma \boldsymbol{u}\, dp, \qquad \forall \boldsymbol{U} \in \boldsymbol{\mathcal{V}},$$

where $\boldsymbol{u} = U \circ X^{-1}$ ($\boldsymbol{U} = \boldsymbol{u} \circ X$) and div_Γ is the surface divergence *defined in the previous section. If X is piecewise C^2 we have the alternative expression*

$$J'(X)[\boldsymbol{U}] = \int_\Gamma H\ (\boldsymbol{n} \cdot \boldsymbol{u})\, dp, \tag{8}$$

where H is the mean curvature function of Γ, and $\boldsymbol{n}$ the unit normal vector field.

It is thus easy to see that every surface of minimal area is a solution to the Plateau problem, which is defined as the problem of finding a surface with a given boundary and $H \equiv 0$. Such surfaces are called *minimal surfaces*. In terms of parametrizations, this is equivalent to finding $X \in \mathcal{S}(\gamma)$ with $H = 0$. With a slight abuse of notation we will call such parametrizations X minimal surfaces.

Remark 3.2 *(Existence and uniqueness).* The minimal surface problem has been one the most celebrated problems in the calculus of variations and there are thousands of works on the subject. The literature has been so fruitful mainly due to the lack of a simple result that would cover most cases. A quick look at [3, Chapter 4] would provide several results on the matter. Even for very simple setups, we can have a singular behavior, such as existence of multiple minimal surfaces. For example if the boundary consists of two circles, not too far apart, there are two different solutions (the catenoid and two separated discs). In the context of this paper we assume that we are approximating a problem for which there exists a minimal surface that has the same boundary and topology of the initial surface we provide, and that it is close to this initial surface.

3.2. Prescribed curvature problem

We have seen that minimizing the area functional led to the problem of finding zeros of another functional F, which are surfaces of vanishing mean curvature. The functional F can be simply generalized so that its zeros are surfaces of a given prescribed mean curvature. This problem makes sense on its own even if the solutions are not minimizers of some functional. More precisely, we now define the functional F whose zeros are surfaces of prescribed constant mean curvature; the minimal surface problem is thus a particular case.

Definition 1 *(Prescribed curvature functional).* Let C be a given constant and define the prescribed curvature functional $F : \mathcal{S}(\gamma) \to \boldsymbol{\mathcal{V}}'$ by

$$F(X)[\boldsymbol{U}] = \int_\Gamma (H - C)\ (\boldsymbol{n} \cdot \boldsymbol{u}) \qquad \text{for all } \boldsymbol{U} \in \boldsymbol{\mathcal{V}}, \quad X \in \mathcal{S}(\gamma),$$

where $\Gamma = X(\Omega)$, $\boldsymbol{u} = \boldsymbol{U} \circ X^{-1}$, H is the mean curvature of Γ and $\boldsymbol{n}$ the normal vector field of Γ.

Our goal is to find a zero of the functional F in the following sense:

Definition 2 *(Prescribed curvature problem).* Let F be the functional from Definition 1, then the prescribed mean curvature problem reads: Find $X^* \in \mathcal{S}(\gamma)$ such that

$$F(X^*)[\boldsymbol{U}] := \int_\Gamma (H - C)(\boldsymbol{u} \cdot \boldsymbol{n}) = 0 \qquad \text{for all } \boldsymbol{U} \in \boldsymbol{\mathcal{V}}. \tag{9}$$

4. Fixed point algorithm

We want to define a Newton-type algorithm to approximate the solutions of the prescribed mean curvature problem, i.e., find the zeros of F from Definition 1. With this goal in mind, we need to find the derivative of F.

Lemma 4.1 *(Derivative of F). Given $X \in \mathcal{R}^m(\Omega)$ and $\Gamma = X(\Omega)$,*

$$F'(X)[\boldsymbol{U}][\boldsymbol{V}] = \int_\Gamma D_\Gamma \boldsymbol{u}^T \boldsymbol{n} \cdot D_\Gamma \boldsymbol{v}^T \boldsymbol{n} + div_\Gamma \boldsymbol{u}\, div_\Gamma \boldsymbol{v} - D_\Gamma \boldsymbol{u}\, \Pi \cdot \Pi\, D_\Gamma \boldsymbol{v}^T + C \int_\Gamma \boldsymbol{u} \cdot D_\Gamma \boldsymbol{v}^T \boldsymbol{n} - (\boldsymbol{u}\cdot\boldsymbol{n}) div_\Gamma \boldsymbol{v}, \qquad \text{for all } \boldsymbol{U}, \boldsymbol{V} \in \boldsymbol{\mathcal{V}}, \tag{10}$$

where $\boldsymbol{n}$ is the normal to Γ.

We postpone the proof of this lemma to the appendix.

4.1. Newton method

A first attempt to find a zero of $F(X)$ is a direct application of Newton method on problem (9), namely, starting with the given X^0 let $k = 0$ and

(1) Let $\boldsymbol{\delta}^k \in \boldsymbol{\mathcal{V}}$ be the solution of $F'(X^k)[\boldsymbol{\delta}^k] = -F(X^k)$
(2) Let $X^{k+1} = X^k + \boldsymbol{\delta}^k$.
(3) Increase k and go to (1).

This method does not work in general regardless of how close X^0 is to X^*. The reason is that $F'(X)$ is not invertible in general, especially when X is very close to a minimal surface. An example illustrating this fact is presented in the appendix (see Proposition A.6). The reason behind the non-invertibility of $F'(X)$ is that we consider all *movements* of the surface, including tangential ones. The latter do not change the surface with infinitesimal steps.

In the next section we propose a modification which only takes into account normal perturbations.

4.2. Modified Newton method

We start this section observing that problem (9) is equivalent to the following:

$$\text{Find } X^* \in \mathcal{S}(\gamma) \text{ such that} \quad F(X^*)[\Psi \boldsymbol{N}^*] = 0 \quad \forall \Psi \in \mathcal{V}, \tag{11}$$

where $\boldsymbol{N}^* = \boldsymbol{N}_{X^*}$ is the pull-back of the normal $\boldsymbol{n}^*$ to the surface $X^*(\Omega)$, and $\mathcal{V}$ is the space of scalar increments defined by

$$\mathcal{V} = \{\Phi \in C^m(\Omega; \mathbb{R}) : \Phi|_{\partial\Omega} = 0\}.$$

Problem (11) is not yet suitable to be solved by a Newton method, but we can still use a Taylor formula approach.

Suppose we have a surface $X \in \mathcal{S}(\gamma)$ with normal $\boldsymbol{N}$ and that it is so close to X^* that $X^* = X + \Phi \boldsymbol{N}$ for some $\Phi \in \mathcal{V}$. Then, problem (11) can be written as:

$$\text{Find } \Phi \in \mathcal{V} \text{ such that} \qquad F(X + \Phi \boldsymbol{N})[\Psi \boldsymbol{N}^+] = 0 \quad \forall \Psi \in \mathcal{V},$$

where $\boldsymbol{N} = \boldsymbol{N}_X$ and $\boldsymbol{N}^+ = \boldsymbol{N}_{X+\Phi\boldsymbol{N}}$.

We now use Taylor's formula to approximate this problem by the following:

$$\text{Find } \Phi \in \mathcal{V} \text{ such that} \qquad F(X)[\Psi \boldsymbol{N}^+] + F'(X)[\Phi \boldsymbol{N}][\Psi \boldsymbol{N}^+] = 0 \quad \forall \Psi \in \mathcal{V}, \tag{12}$$

where we still denote $\boldsymbol{N}^+ = \boldsymbol{N}_{X+\Phi\boldsymbol{N}}$.

This problem, in turn, can be approximated by the more explicit, linear problem

$$\text{Find } \Phi \in \mathcal{V} \text{ such that} \qquad F'(X)[\Phi \boldsymbol{N}][\Psi \boldsymbol{N}] = -F(X)[\Psi \boldsymbol{N}] \quad \forall \Psi \in \mathcal{V},$$

which is obtained from (12), replacing $\boldsymbol{N}^+$ by $\boldsymbol{N} = \boldsymbol{N}_X$.

We use this equation to build an iterative scheme at the continuous level.

Algorithm 1 *(Continuous scheme).* Let P be a projection from C^{m-1} to C^m. Let $X^0 \in \mathcal{R}^m(\Omega)$ be some initial surface defining $\mathcal{S}(\gamma)$. We then set $k = 0$ and define a sequence of surfaces in $\mathcal{S}(\gamma)$ as follows:

(1) Find $\Phi^k \in \mathcal{V}$ such that $F'(X^k)[\Phi^k \boldsymbol{N}^k][\Psi \boldsymbol{N}^k] = -F(X^k)[\Psi \boldsymbol{N}^k]$, $\forall \Psi \in \mathcal{V}$, where $\boldsymbol{N}^k$ denotes the normal to $\Gamma^k = X^k(\Omega)$.
(2) Let $X^{k+1} = X^k + P(\Phi^k \boldsymbol{N}^k)$.
(3) Increase k and go to step (1).

In the definition of Algorithm 1, it is not necessary to restrict to one specific projection. In our simulations we have used an L^2 projection. Also for the implementation of this algorithm, it is worth observing the simplified form that $F'(X)[\cdot][\cdot]$ from (10) takes when considering only normal perturbations.

Proposition 4.2 *(Derivative for normal perturbations). If $X \in \mathcal{R}^m(\Omega)$ with $m \geq 2$, then*

$$F'(X)[\Phi \boldsymbol{N}][\Psi \boldsymbol{N}] = \int_\Gamma \nabla_\Gamma \phi \cdot \nabla_\Gamma \psi + \int_\Gamma (2K - CH)\phi\psi, \quad \text{for all } \Phi, \Psi \in \mathcal{V}, \tag{13}$$

where ϕ and ψ are the push-forward of Φ and Ψ, respectively.

The proof of this proposition can be found in the appendix.

Remark 4.3. It is worth mentioning that one could also compute surfaces of prescribed mean curvature by minimizing the functional $\int (H - C)^2$, instead of finding zeros of the functional F from Definition 1. The method developed in this article aims at finding zeros of functionals with a Newton-type algorithm, in order to obtain quadratic convergence. Solving such a minimization problem with these techniques would require computing second order derivatives of the functional. A descent algorithm would allow us to start from a not so close initial surface, but would lead to linear convergence. It seems that a combination of both techniques should be the best choice; we will work on this idea in a forthcoming article.

4.3. A more general setting

The method generalizes naturally to surfaces that cannot be parametrized by a single patch and to dimension greater than three. Let the initial regular surface Γ^0 in $\mathbb{R}^{n+1}$ be given with boundary $\gamma = \partial\Gamma^0$. The method recursively generates from the surface Γ^k a new surface Γ^{k+1} as follows. Let

$$\begin{aligned} \mathcal{S}^k(\gamma) &= \{X : \Gamma^k \to \mathbb{R}^{n+1} : X|_\gamma = \mathrm{id}^k \\ &\qquad \text{and } X \text{ is a } C^m \text{ diffeomorphism onto } X(\Gamma^k)\} \\ \mathcal{V}^k &= \{\Phi : \Gamma^k \to \mathbb{R} : \Phi|_\gamma = 0 \text{ and smooth}\} \\ F^k(X)[V] &:= \int_{X(\Gamma^k)} (H - C)v, \qquad \forall V \in \mathcal{V}_0^k, \\ &\qquad \text{where H is the mean curvature of } X(\Gamma^k), \end{aligned} \tag{14}$$

then we let $X_k = id^k + P(\Phi^k \boldsymbol{N}^k)$ where Φ^k is the solution of

$$(F^k)'(id^k)[\Phi^k \boldsymbol{N}^k][\Psi \boldsymbol{N}^k] = -(F^k)(id^k)[\Psi \boldsymbol{N}^k], \quad \forall \Psi \in \mathcal{V}^k,$$

and P^k is a projection onto $C^m(\Gamma^k)$. Then $\Gamma^{k+1} = X^k(\Gamma^k)$.

Remark 4.4 *(Convergence).* In the following section we propose a discrete scheme for Algorithm 1 based on B-splines and present numerical evidence (through its implementation in a variety of examples) supporting the convergence properties of the method. The question on the mathematical assumptions that would imply the convergence of the method is an open problem that we are investigating at the moment.

5. Discretization

We want to adapt Algorithm 1 to a discrete setting using spaces of high regularity, namely isogeometric spaces. These are spaces constructed from tensor product splines. In this section we briefly describe them and present the discrete algorithm.

5.1. B-splines and NURBS

5.1.1. Univariate B-spline

Given a non-negative number p, a *spline* of degree p on the interval $[a, b]$ is a real valued piecewise polynomial function of degree at most p on each subinterval of $[a, b]$ determined by the partition $a = \zeta_1 < \cdots < \zeta_m = b$. The ζ_i's are called the *knots* and they form the *knot vector* $\boldsymbol{\zeta} = (\zeta_1, \ldots, \zeta_m)$. At each knot, the spline function is allowed to have a regularity that ranges from discontinuous (C^{-1}) to C^{p-1}, this is usually indicated using the so called *regularity vector* $\boldsymbol{\alpha} = (\alpha_1, \ldots, \alpha_m)$ where $\alpha_i \in \mathbb{Z}$ and $-1 \leq \alpha_i \leq p-1$. It is sometimes convenient to encode both knot and regularity vectors into a single vector

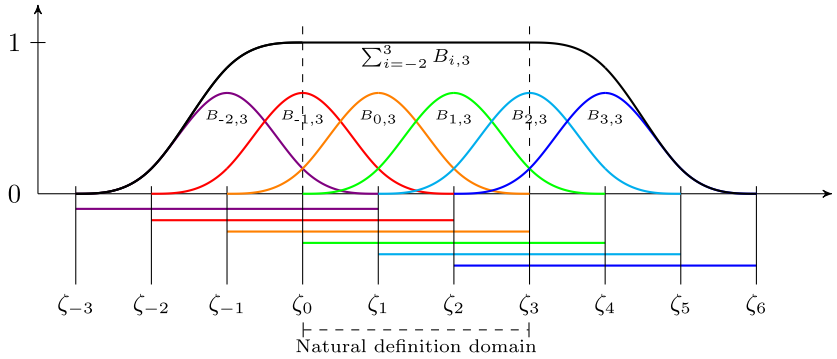

Fig. 1. One dimensional B-spline basis functions of degree 3 for a maximum regularity knot vector. As can be seen, all the functions are non-negative; they span over four knot intervals (small support); on each interval only four functions have non-zero values; and they form a partition of unity on the interval $[\zeta_0, \zeta_3]$.

of repeated knots $\boldsymbol{\xi} = (\underbrace{\zeta_1, \ldots, \zeta_1}_{r_1 \text{ times}}, \underbrace{\zeta_2, \ldots, \zeta_2}_{r_2 \text{ times}}, \ldots, \underbrace{\zeta_m, \ldots, \zeta_m}_{r_m \text{ times}})$, where $r_i = p - \alpha_i$, and $\boldsymbol{r} = (r_1, \ldots, r_m)$ is called the *multiplicity vector*. When the multiplicity of the first and last knots is $p+1$ we call $\boldsymbol{\xi}$ an *open knot vector*.

We define $S^p_{\boldsymbol{\xi}}$ to be the space of spline functions of degree p subordinated to the knot vector with repetition $\boldsymbol{\xi}$. It is a well known result that the dimension of this space is $n = \sum_{i=1}^{m} r_i - p - 1$. The classical Cox–de Boor recursive algorithm [13] allows to construct a basis for $S^p_{\boldsymbol{\xi}}$, known as the B-spline basis. We denote these basis functions by B_i (see Fig. 1). Some important properties of B-spline basis functions are:

1. *Non-negativity*: each $B_i(x) \geq 0$ for all $x \in [a, b]$.
2. *Small support*: the support of B_i is contained in $[\xi_i, \xi_{i+p+1})$, and on each interval $[\zeta_i, \zeta_{i+1})$ (with $i = 1, \ldots, m-1$), only $p+1$ basis functions have non-zero values.
3. *Partition of unity*: the set of basis functions $\{B_1, \ldots, B_n\}$ satisfies that $\sum_{i=1}^{n} B_i(x) = 1$, for all $x \in [a, b]$ if $\boldsymbol{\xi}$ is an open knot vector.

5.1.2. Bivariate B-splines

The univariate spline spaces can be used to generate multidimensional spline spaces through tensor products. For this work we just consider the bivariate case. More precisely, given $d = 2$ we consider the spline spaces $S^{p_i}_{\boldsymbol{\xi}_i}([a_i, b_i])$ for $i = 1, 2$ and define the bivariate spline space $S^{p_1,p_2}_{\boldsymbol{\xi}_1,\boldsymbol{\xi}_2}(\hat{\Omega}) = S^{p_1}_{\boldsymbol{\xi}_1}([a_1, b_1]) \otimes S^{p_2}_{\boldsymbol{\xi}_2}([a_2, b_2])$, where $\hat{\Omega}$ is the rectangle $[a_1, b_1] \times [a_2, b_2]$. In this case the bivariate B-Spline basis functions are

$$B_{i_1,i_2}(x_1, x_2) = B^1_{i_1}(x_1) B^2_{i_2}(x_2) \tag{15}$$

with $B^i_j \in S^{p_i}_{\boldsymbol{\xi}_i}$, $j = 1, \ldots, n_i$ being the B-spline basis functions of the univariate spaces. The dimension of the space is $n = n_1 \times n_2$.

5.1.3. Vector valued B-splines

Given an integer s we define the vector valued spline space $\boldsymbol{S}^s$ to be the set of all vector valued functions $\hat{\boldsymbol{\phi}} : \hat{\Omega} \to \mathbb{R}^s$ such that $\hat{\boldsymbol{\phi}} \cdot e_i \in S^{\boldsymbol{p}_i}_{\boldsymbol{\xi}_i}$.

5.2. Isogeometric spaces

The isogeometric spaces are spaces constructed by providing:

1. **A reference space**. This is a tensor product spline or NURBS space with a rectangle as domain.
2. **A deformation**. Provides a smooth deformation or mapping $\boldsymbol{F} : \hat{\Omega} \to \mathbb{R}^s$ (with smooth inverse). $\Omega = \boldsymbol{F}(\hat{\Omega})$.
3. **A transformation type**. This is a rule that specifies how to use the deformation to transform the functions in the reference space into the ones in the physical space. Some example besides direct composition are divergence and curl preserving transformations (cf. Table 1).

5.3. Discrete algorithm

Recall that m is a parameter for the regularity of the spaces that we consider given and fixed. The discrete algorithm is obtained by replacing the set $\mathcal{S}(\gamma)$ appearing in Algorithm 1. More precisely, let S_h and $\boldsymbol{S}_h$ be the scalar-valued and vector-

Table 1
Examples of different transformation types to obtain a physical discrete space $\mathbb{V}$ from a reference spline or NURBS space $\hat{\mathbb{V}}$ and a mapping $\boldsymbol{F}$. The table shows the transformation name given in the library and the formula that defines its push-forward operator.

h_grad	h_curl	h_div	l_2
$\phi = \hat{\phi} \circ \boldsymbol{F}^{-1}$	$\boldsymbol{u} = D\boldsymbol{F}^{-T}(\hat{\boldsymbol{u}} \circ \boldsymbol{F}^{-1})$	$\boldsymbol{v} = \frac{D\boldsymbol{F}}{\det D\boldsymbol{F}}(\hat{\boldsymbol{v}} \circ \boldsymbol{F}^{-1})$	$\Phi = \frac{\hat{\Phi} \circ \boldsymbol{F}^{-1}}{\det D\boldsymbol{F}}$

Table 2
The high regularity of the isogeometric spaces allows us to compute the curvature of the approximation directly, this in turn gives means to consider the following norms to measure the approximation quality to the minimal surface, even if we don't know the exact solution.

Mean error	L^1 error	L^2 error	L^∞ error
$\left\lvert \frac{1}{\lvert\Gamma\rvert} \int_\Gamma H - C \right\rvert$	$\frac{1}{\lvert\Gamma\rvert} \int_\Gamma \lvert H - C \rvert$	$\left(\frac{1}{\lvert\Gamma\rvert} \int_\Gamma \lvert H - C \rvert^2 \right)^{1/2}$	$\lVert H - C \rVert_{L^\infty(\Gamma)}$

valued bi-variate spline spaces of degree $p = m + 1$ and maximum regularity respectively. The subscript h is a parameter indicating the knot spacing, also called mesh size. Now we can state the discrete scheme.

Algorithm 2 *(Discrete scheme).* Let P_h be a chosen projection from C^{m-1} to $\boldsymbol{S}_h$. Let $X^0 \in \mathcal{R}^m(\Omega)$ be a given initial surface fixing the boundary and thus defining the admissible set $\mathcal{S}(\gamma)$. Define:

- $X_h^0 := P_h(X^0)$
- $\mathcal{S}_h(\gamma) := \{X \in \boldsymbol{S}_h \cap \mathcal{R}^m(\Omega) : (X - X_h^0)|_{\partial\Omega} = 0\}$
- $\mathcal{V}_h := \{\Phi \in S_h : \Phi|_{\partial\Omega} = 0\}$

and generate for $k = 0, 1, 2, \ldots$ the sequence of surfaces in $\mathcal{S}_h(\gamma)$ recursively, as follows:

1. Find $\Phi^k \in \mathcal{V}_h$ such that

$$F'(X_h^k)[\Phi^k \boldsymbol{N}^k][\Psi \boldsymbol{N}^k] = -F(X_h^k)[\Psi \boldsymbol{N}^k] \; \forall \Psi \in \mathcal{V}_h$$

2. Let $X_h^{k+1} := X_h^k + P_h(\Phi^k \boldsymbol{N}^k)$.

6. Examples

In this section we present a number of numerical simulations using the discrete scheme described in Algorithm 2. The purpose is to show experimentally the stability and convergence properties of the method under a variety of situations.

To run the simulations below, Algorithm 2 was implemented using the software library `igatools` [8]. This open source C++ library allows, among other things, the use of vector-valued and periodic isogeometric spaces. To solve the symmetric linear system we employed a preconditioned conjugate gradient algorithm. The simulations were run on a desktop computer with 4 cores.

The discrete spaces are tensor product splines with maximum regularity for a chosen degree p, namely they are C^m with $m = p - 1$. Given the possibility of using a high regularity for the solution spaces, it is simple to compute the curvature of the approximation directly—which is not the case if we use the usual (C^0) finite element spaces. This fact can be exploited, among other things, to have a good measure of the approximation error to the exact solution even if the latter is not known. More precisely, as a minimal surface has zero mean curvature (or constant in the case of prescribed curvature) we can measure how close the approximation is to the exact solution by measuring its curvature, even if we don't know the exact solution. If we denote by Γ the surface obtained in the approximation and by H its mean curvature, which we can evaluate point wise thanks to the high regularity of the space, and if C denotes the prescribed constant curvature ($C = 0$ for a minimal surface) we can consider different norms to measure the approximation quality to the minimal surface, shown in Table 2. Moreover the curvature involves up to second order derivatives, which are also included in the natural norm used to define F'.

The simulations exhibit a fast convergence of the method, in less than 5 iterations the surface is indistinguishable to the eye from the exact surface. The same behavior is observed regardless of the resolution, whether 100 or 10000 degrees of freedom were used. These observations are consistent with a fixed point method of Newton type. Also, as expected from this type of methods, it is necessary to start with an initial surface which is not too far away from the expected solution. Since F' involves the mean curvature H of the surface, this closeness must be measured with norms involving up to second order derivatives.

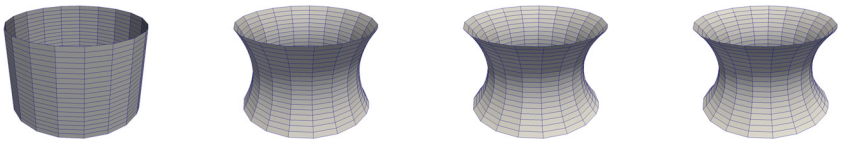

Fig. 2. Algorithm 2 is applied to an initial cylinder of radius 1.6 and height 2. The sequence illustrates the initial surface followed by the first three iterations. The fourth iteration (not shown) is indistinguishable from the third to the naked eye. For this simulation the spline space used is periodic of degree 3, giving a C^2 regularity for the solution. Convergence results both in terms of the space polynomial degrees and number of knots for this problem are provided in Tables 3 and 4.

Table 3
Curvature error for different norms (cf. Table 2) with the experimental order of convergence in terms of the element size h. The simulation correspond to the cylinder to catenoid problem illustrated in Fig. 2, with C^2 splines of degree 3. Notice that the experimental order of convergence fits the expected one from the theory of approximation with splines.

h	Mean error		L^1 error		L^2 error		L^∞ error	
$\frac{1}{3}$	2.39e−03	–	2.32e−01	–	2.63e−01	–	6.63e−01	–
$\frac{1}{6}$	1.49e−04	4.00	3.23e−02	2.85	3.55e−02	2.89	8.40e−02	2.98
$\frac{1}{12}$	2.04e−05	2.87	6.92e−03	2.22	7.58e−03	2.23	1.86e−02	2.17
$\frac{1}{24}$	2.47e−06	3.05	1.66e−03	2.05	1.82e−03	2.06	4.59e−03	2.02
$\frac{1}{48}$	3.01e−07	3.04	4.13e−04	2.01	4.52e−04	2.01	1.40e−03	1.71

Table 4
L^2 error of mean curvature and experimental order of convergence in terms of the mesh size h for different polynomial degrees. The simulations are for the cylinder to catenoid problem illustrated in Fig. 2. From the theory of approximation by splines the expected order for the error in H^2 norm, which bounds the L^2-norm of the curvature error is $p-1$ when using splines of degree p; this is perceived in the table. Observe that the higher the degree the faster the error decreases, for example the same error attained using degree 2 and 192 knots is the same as the one attained using degree 4 with 6 knots.

h	Degree 2		Degree 3		Degree 4	
$\frac{1}{3}$	5.51e−01	–	2.63e−01	–	1.12e−01	–
$\frac{1}{6}$	9.82e−02	2.49	3.55e−02	2.89	4.69e−03	4.58
$\frac{1}{12}$	2.68e−02	1.87	7.58e−03	2.23	2.75e−04	4.09
$\frac{1}{24}$	9.42e−03	1.51	1.82e−03	2.06	3.97e−05	2.80
$\frac{1}{48}$	4.09e−03	1.20	4.52e−04	2.01	–	–
$\frac{1}{96}$	1.96e−03	1.06	–	–	–	–
$\frac{1}{192}$	9.71e−04	1.01	–	–	–	–

6.1. Catenoid

As a first example we consider the catenoid, which was the first non-planar minimal surface to be discovered, and arises by rotating a catenary about an axis (its directrix); it is thus not homeomorphic to a disc. The boundary of this surface is the union of two circles of equal radius with centers at the directrix and lying in parallel planes perpendicular to the axis. In order to obtain this surface with our method we consider a cylinder as the initial surface. Fig. 2 shows some iterations of the method, starting with a cylinder of radius 1.6 and height 2, using a spline space of degree 3 with C^2 regularity.

Using the error measures proposed at the beginning of this section (see Table 2), Tables 3 and 4 present the experimental convergence rates obtained in terms of the mesh size and polynomial degree, respectively. The mesh size, denoted by h in Table 3, is the diameter of the elements in the reference domain, where uniform partitions were used. Table 3 shows how the curvature error decreases as we halve the mesh size, for different norms. Notice that the experimental order of convergence fits the expected one from the theory of approximation with splines; using degree 3 we expect the H^2 norm of the error to be of order 2. Similarly, in Table 4, we show how the L^2-error of the curvature behaves for different degrees of the spline spaces. Also here the expected order of convergence expected by the theory is verified. Observe that the higher the degree the faster the error decreases; for example, the same error is attained using degree 2 and 192 knots and using degree 4 with 6 knots. The simulations were carried out until it was possible for the given machine precision.

We also obtained a catenoid when taking a truncated cone as the initial surface, where the two circular components of the boundary are of different radius. This situation is shown in Fig. 3. Starting from a truncated cone (upper radius 1.6, lower radius 3 and height 3) Algorithm 2 quickly converges to a catenoid, and the expected orders of convergence are observed for this simulation, even though not reported.

Fig. 3. A catenoid approximation is also obtained (cf. Fig. 2) if Algorithm 2 is applied to an initial truncated cone. The sequence illustrates the initial surface followed by the first two iterations. The third iteration (not shown) is indistinguishable from the second to the naked eye. In this simulation the initial cone dimensions are: upper radius 1.6, lower radius 3 and height 3. The spline space used is periodic of degree 3, with 30 knots in each direction. Similar order of convergence as of Table 4 were also obtained in this case.

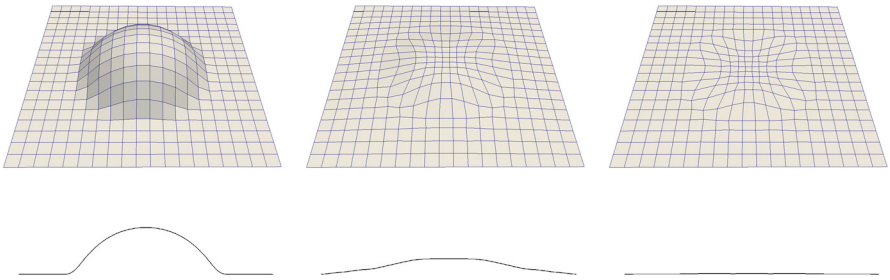

Fig. 4. Algorithm 2 is applied to an initial (axisymmetric) bump on a rectangular region. The sequence illustrates the initial surface followed by the first two iterations. After three iterations of the method the surface is numerically flat. For this simulation the initial surface is the graph of the function $f(x,y) = \frac{3}{2} e^{-\frac{1}{1-x^2-y^2}} \chi_{\{x^2+y^2<1\}}$ defined in a square $R = [-1.5, 1.5] \times [-1.5, 1.5]$ and the spline space used is of degree 3 with 20 knots per direction. A non-axisymmetric perturbation is considered in Fig. 5.

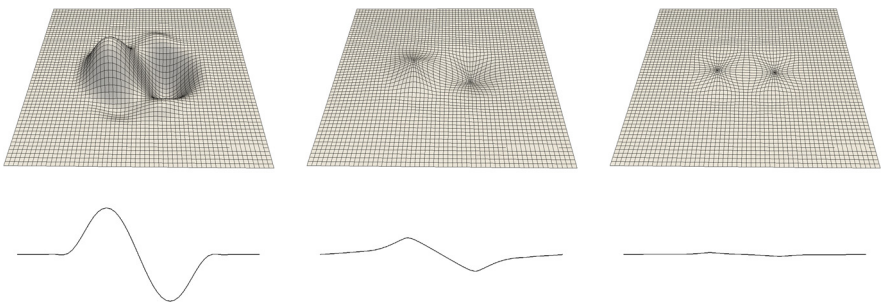

Fig. 5. Algorithm 2 is applied to an initial perturbation on a rectangular region. The sequence illustrates the initial surface followed by the first two iterations. After three iterations of the method the surface is numerically flat. For this simulation the initial surface is the graph of the function $f(x,y) = \frac{3}{2} e^{-\frac{1}{1-x^2-y^2}} \cos(\pi x) \sin(\pi x) \chi_{\{x^2+y^2<1\}}$ defined in a square $R = [-1.5, 1.5] \times [-1.5, 1.5]$ and the spline space used is of degree 3 with 20 knots per direction. In this graph z axis is rescaled by a factor 2.

6.2. Planar regions

Another instance for which we know the minimal surface is when the boundary curve lies on a plane. In order to test this situation with our numerical method we fed Algorithm 2 with an initial surface consisting of a perturbation of a plane region. In Figs. 4 and 5 we can see the evolution of two different perturbations of a rectangular region to the rectangle in three iterations.

It is interesting to observe that even though in three iterations we have reached the geometry of the plane, the knot lines in the plane are not straight. This happens because the surface is updated using normal increments and not vertically as a graph. This mesh *degeneration* may lead to non-convergence in some situations and should be taken into account when designing improvements of the algorithm, such as mesh regularizations (see Section 7).

We have also observed that considering different initial surfaces, keeping the height of the bump fixed while decreasing its support we reach a configuration where Algorithm 2 ceases to converge. This is explained by the fact that the distance between the initial surface and the minimal surface must be small in a strong sense, considering also curvatures (or second order derivatives), in order to achieve convergence. If the height of the bump is kept fixed while decreasing the support, what we are actually doing is increasing its curvature moving it further away form the expected solution of zero mean curvature. What usually happens in this situation is that at a certain step, the image of $X_h^{k+1} := X_h^k + P_h(\Phi^k \boldsymbol{N}^k)$ is not a surface because it presents self-intersections (see Fig. 6).

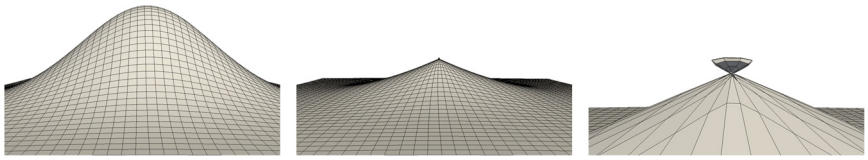

Fig. 6. In this case, Algorithm 2 produces a self-intersected surface in the first iteration. For this simulation the initial surface is the graph of the function $f(x, y) = e^{-x^2-y^2}$ defined in a square $R = [-2, 2] \times [-2, 2]$ and the spline space used is of degree 3 with 20 knots per direction. The third image is a zoom over the self-intersection zone.

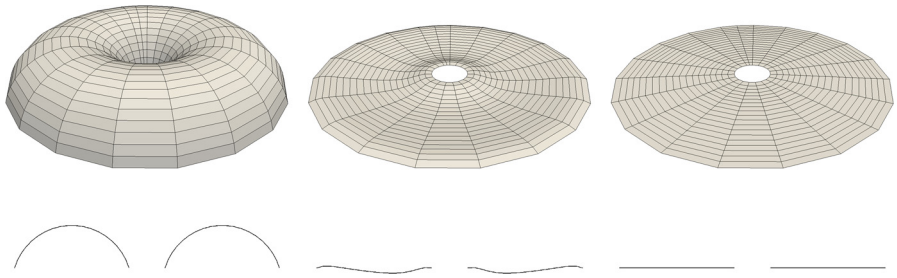

Fig. 7. Algorithm 2 is applied to an initial upper half of a torus, whose boundary lies on the plane. The sequence illustrates the initial surface followed by the first two iterations. The third iteration (not shown) is indistinguishable from the second to the naked eye. For this simulation the spline space used is of degree 3, with maximum regularity (C^2). In this graph, the z axis is rescaled by a factor 2.

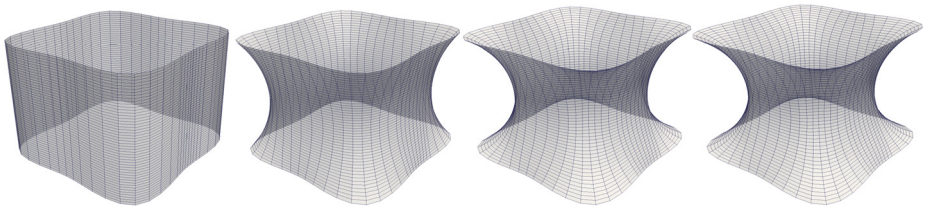

Fig. 8. Algorithm 2 is applied to an initial polyhedral surface of four sides. The polyhedron has infinite curvature at the edges but the projection of the algorithm makes it a C^m surface. The sequence illustrates the projected initial surface followed by the first three iterations. The fourth iteration (not shown) is indistinguishable from the third to the naked eye. For this simulation, C^2 splines of degree 3 were used. Notice that using finer mesh size would change the initial surface X_0 and also the boundary.

Another instance of plane perturbation is shown in Fig. 7. Here starting from half a torus (i.e. a surface of revolution whose boundary are two concentric circles in the same plane) the algorithm reaches a ring in the plane.

6.3. Minimal surfaces with singularities

To further investigate the numerical aptitudes of Algorithm 2 we study its behavior when the starting surface has some singularity, for example we propose to use a polyhedral surface (the lateral side of a box) as the initial guess. The polyhedron has infinite curvature at the edges but the projection of the algorithm makes it a C^m surface. Fig. 8 illustrates some iterations for this case. Notice that if the initial surface is not regular (as for the box over its edges) Algorithm 2 uses a projection that would still provide an initial regular surface. The finer the mesh, the higher the curvature will be at the regions around the singular edges of the original box. Clearly in this case the H^2 norm of the initial guess goes to infinity on the edges as the mesh size decreases. Therefore, when h is very small, the initial guess is far from the minimal surface, and the algorithm fails to converge.

Another type of singularity may occur when the starting surface is smooth but it's boundary is not. An example is a "square" piece of a sphere (see Fig. 9). Here the curvature at the corner points of the boundary will not change as long as the boundary is not changed, because the curvature along two linearly independent directions is fixed. Regardless of the surface we consider for this boundary the mean curvature at the corners is given, and nonzero in the example. Nevertheless, Algorithm 2 still converges and the resulting surface is a minimizer of the area functional, but the mean curvature is not zero near the singular points of the boundary, for the discrete surface. The exact minimal surface will have a discontinuous mean curvature, which will vanish at the interior of the surface. Figs. 9 and 10 show some iterations starting from a piece of sphere and sinusoidal ribbon.

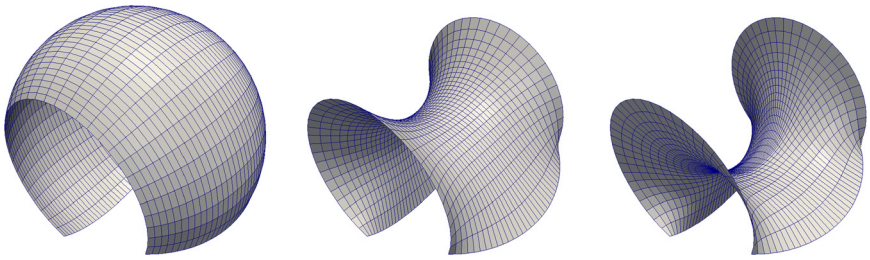

Fig. 9. Algorithm 2 is applied to an initial spherical piece (smooth). The boundary is not smooth as it presents four corners which have a given curvature. The sequence illustrates the initial surface followed by iterations 2 and 5. The sixth iteration (not shown) is indistinguishable from the fifth to the naked eye. For this simulation the spline space used is of degree 3.

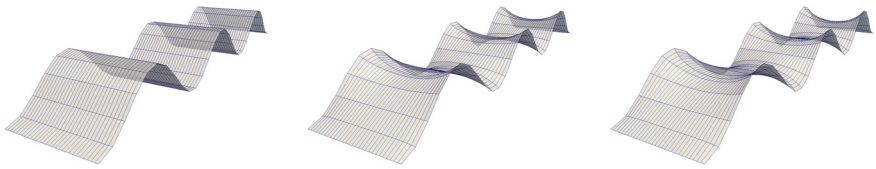

Fig. 10. Initial surface: ruled surface obtained joining two parallel trigonometric curves. The solution is area minimizer but has nonzero curvature near the edges.

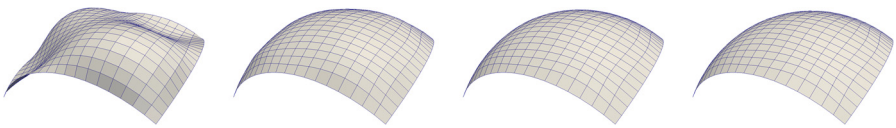

Fig. 11. The left frame in the figure is an initial undulating surface with a spherical boundary. This boundary belongs to a sphere of radius 1. Algorithm 2 is then applied to this surface with a prescribed constant curvature parameter $C = 2$. The sequence illustrates the initial surface followed by the first two iterations. After two iterations of the method the surface is indistinguishable to the naked eye from a sphere of radius 1. For this simulation the initial surface is given by the parametrization $X(s,t) = r(s,t)\cos s \sin t\boldsymbol{i} + r(s,t)\sin s \sin t\boldsymbol{j} + r(s,t)\cos t\boldsymbol{k}$, where $r(s,t) = R(1+\epsilon(s-a)(b-s)(s-\frac{a+b}{2}))$, $R = 1$ and $\epsilon = 10$. X is defined for $(s,t) \in [a,b]\times[c,d]$, where $a = 0, b = \pi/2, c = \pi/3$ and $d = 2\pi/3$. The spline space used is of degree 3 with 20 knots per direction. Convergence rates for this problem are given in Tables 5 and 6.

Table 5
Curvature error for different norms (cf. Table 2) with the experimental order of convergence in terms of the mesh size h. The simulations correspond to the undulating manifold with spherical boundary problem illustrated in Fig. 11. Similar to the situation of minimal surfaces, in the case of constant prescribed mean curvature we observe that the experimental order of convergence fits the expected one from the theory of approximation with splines. Here the polynomial degree is 3, thus the expected approximation order for the H^2 norm is 2. Table 6 shows convergence rates in terms of the mesh size h and spline polynomial degree.

Knots	Mean error		L^1 error		L^2 error		L^∞ error	
$\frac{1}{3}$	1.96e−01	–	5.88e−01	–	7.64e−01	–	2.43	–
$\frac{1}{6}$	3.21e−02	2.61	1.30e−01	2.17	2.03e−01	1.91	1.56	0.64
$\frac{1}{12}$	3.72e−03	3.11	2.71e−02	2.26	4.67e−02	2.13	4.07e−01	1.94
$\frac{1}{24}$	4.52e−04	3.04	6.70e−03	2.02	1.11e−02	2.07	1.04e−01	1.96
$\frac{1}{48}$	5.54e−05	3.03	1.68e−03	2.00	2.70e−03	2.04	2.63e−02	1.99

6.4. Surfaces of prescribed mean curvature

In this work we only deal with the case of constant mean curvature (cf. Section 7). Two well known surfaces of constant mean curvature are a sphere of radius R, with mean curvature $\frac{2}{R}$ and a cylinder of radius R with mean curvature $\frac{1}{R}$.

In the first example we start with a piece of a sphere that has been previously distorted in the interior by an undulating deformation. The boundary of this surface belongs to a sphere of radius $R = 1$. Then we set the prescribed curvature $C = \frac{2}{R} = 2$ and let Algorithm 2 proceed. In Fig. 11, we show some iterations of the method. In two iterations the surface is indistinguishable to the eye from a sphere of radius 1. A more quantitative measure of the convergence is provided in Table 5 that shows the convergence rates for different norms in terms of the mesh size h and Table 6 that gives the convergence rates in terms of h for different spline polynomial degree. Similar to the situation of minimal surfaces, in this case of constant prescribed mean curvature we observe that the experimental order of convergence fits the expected one from the theory of approximation with splines.

In the next example we start with a cylinder of radius R and height 2ℓ. The boundary consists of two parallel circles of radius R distant apart by 2ℓ. It not difficult to see that there exists one sphere that contains the boundaries with radius

Table 6
L^2 error of the mean curvature, with the experimental order of convergence in terms of the element size h and spline polynomial degree. The simulations correspond to the undulating manifold with spherical boundary problem illustrated in Fig. 11. From the theory of approximation by splines the expected order to approximate the H^2 norm with splines of degree p is $p-1$, which is numerically verified in the table. Observe that the higher the degree the faster the error decreases, for example the same error is archived using degree 2 and 96 knots as using degree 4 with 6 knots.

h	Degree 2		Degree 3		Degree 4	
$\frac{1}{3}$	8.29e−02	–	7.64e−01	–	3.47e−01	–
$\frac{1}{6}$	4.34e−01	−2.39	2.04e−01	1.91	6.24e−02	2.48
$\frac{1}{12}$	2.22e−01	0.97	4.67e−02	2.13	1.00e−02	2.63
$\frac{1}{24}$	1.09e−01	1.02	1.11e−02	2.07	1.35e−03	2.90
$\frac{1}{48}$	5.45e−02	1.01	2.70e−03	2.04	–	–
$\frac{1}{96}$	2.72e−02	1.00	–	–	–	–
$\frac{1}{192}$	1.36e−02	0.99	–	–	–	–

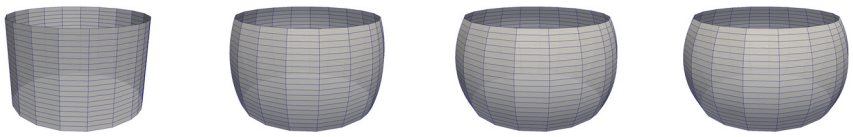

Fig. 12. The left frame in the figure is an initial cylinder radius $R = 1.6$ and height $2l = 2$. The boundary of this cylinder is contained in a sphere of radius $r = \sqrt{l^2 + R^2}$. Algorithm 2 is then applied to this cylinder using a prescribed constant curvature parameter $C = \frac{2}{r}$. The sequence illustrates the initial surface followed by some iterations. In the last iteration shown the surface is indistinguishable from a sphere of radius r. The spline space used is periodic of degree 3 with 20 knots per direction. And the iterations are 1, 3, 10. In Fig. 13 the process is reverted.

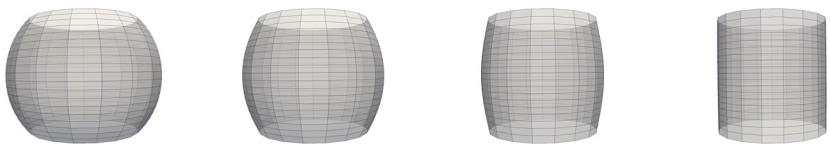

Fig. 13. The left frame in the figure is an initial truncate sphere of radius r. The top and bottom truncation are symmetric forming two boundary circles of radius R and $2l$ distant apart. The cylinder with this same boundary has a mean curvature $\frac{1}{R}$. Algorithm 2 is then applied to spherical initial surface using a prescribed constant curvature parameter $C = \frac{1}{R}$. The sequence illustrates the initial surface followed by some iterations. In the last iteration shown the surface is indistinguishable from a cylinder of radius R and height $2l$. The spline space used is periodic of degree 3 with 20 knots per direction. And the iterations are 1, 3, 9. This simulation is the reverted direction of the one shown in Fig. 12.

$r = \sqrt{\ell^2 + R^2}$. The simulation, illustrated in Fig. 12, consists in using Algorithm 2 starting from the cylinder and setting the prescribed curvature parameter $C = \frac{2}{r}$.

Another associated example is to consider reverting the process of the previous problem. This is, to start from a truncated sphere of radius r and set the prescribed curvature parameter $C = \frac{1}{R}$. The iterations of such example are depicted in Fig. 13, starting from a spherical piece of a sphere of radius r with boundary consisting of two parallel circles of radius R and 2ℓ apart we apply Algorithm 2 setting the prescribed curvature parameter $C = \frac{1}{R}$.

7. Conclusions and future directions

We have developed a Newton type algorithm to approximate parametric surfaces of prescribed constant mean curvature. The algorithm is especially suited to its implementation using isogeometric elements or splines. We described its implementation with C^{m-1} splines of degree m using the isogeometric software library `igatools` [8]. We illustrated its behavior through several examples. The algorithm converges in very few iterations, provided the initial guess is close to the exact solution, not only in Hausdorff distance, but in a distance which involves the curvature, i.e., second order derivatives. When considering a sequence of meshes with decreasing mesh size, the expected rate from approximation theory was observed in all situations, for different polynomial degrees.

If the initial surface is far from the solution, the proposed method will not converge in general. If this is the case some other method (or modification) must be included to provide a good initial surface. If the sought surface is a minimizer of some functional for which a gradient flow is easy to compute, then one can use a gradient flow strategy to generate the initial surface.

We believe that it is possible within the algorithm proposed in this work to specify the “slope” or “contact angle” of the surface on a portion of its boundary. This would be useful for surface tension problems involving droplets on surfaces. For instance, one could have a surface whose boundary is constrained to lie on another surface (the substrate), but is free to move within that surface. One would then need to prescribe the contact angle of the first surface (with respect to the

substrate) on its boundary curve. This would be desirable for simulating equilibrium shapes of droplets interacting with rigid walls (see [14,15]).

We have only presented the algorithm and its motivation, with many examples illustrating its very good performance. A thorough analysis of sufficient conditions guaranteeing convergence will be subject of future research, as are those which we comment below:

Relaxation steps: We intend to develop an algorithm to approach a desired curvature by moving through intermediate curvatures, and should work even for initial surfaces that are far from the exact solution. The idea is to aim at a curvature which is closer to that of the current surface—using the algorithm described here—then update, and repeat.

Reparametrization and regularization: We intend to reparametrize the surface inside the Newton iterations as this idea leads to improvement on the conditioning of the discrete problem. This is a mathematically tractable way of controlling what is usually called mesh smoothing, or moving strategies.

Nonconstant prescribed curvature: The idea is to adapt the algorithm proposed here to allow for approximation of surfaces of prescribed variable mean curvature. It seems that the right problem to study is the case of a prescribed variable mean curvature defined in the embedding space, albeit it is not yet well understood for which variable target curvatures the problem is well posed. Even though the algorithm can be stated in a similar way we need to modify it to incorporate the generation of the initial surface. Notice that our method requires an initial surface that is close to the solution in a norm involving second order derivatives, which in this case means that the variable curvature of the initial surface must be close to the prescribed one. So the issue that we want to address in a different paper is how to adapt the method so as to generate a relaxation path to obtain the sought surface.

Willmore flow and surface diffusion: We plan to design algorithms using isogeometric elements to simulate surface diffusion and Willmore flow, these are nonlinear evolutionary problems where the unknown is a surface which undergoes deformations based on derivatives of its mean and/or Gauss curvature. These equations appear in numerous applications in material science and biology. The ideas behind the algorithm developed here might be useful when leading with the nonlinearities.

Acknowledgements

This work was partially supported by CONICET through grant PIP 112-2011-0100742, by Universidad Nacional del Litoral through grant CAI+D PI 501 201101 00476 LI, and by Agencia Nacional de Promoción Científica y Tecnológica, through grants PICT-2012-2590, PICT-2013-3293 (Argentina).

Appendix A

In this section we collect the more technical proofs of some statements presented in the paper. The following results, except for a counterexample showing the non-invertibility of F', are known (see for example [12,16,17]). For the sake of completeness we have decided to include them here, in an appendix, not to interfere with the flow of ideas in the main part of the manuscript.

A.1. Auxiliary results

We first state some calculus result on surfaces analogous to those in Euclidean spaces such as product formulas and the divergence theorem, which can be easily proved from the definitions (4) and (7).

Lemma A.1 *(Product formulas). Let α, $\boldsymbol{u}$, $\boldsymbol{v}$ and S be smooth fields in Γ, with α scalar valued, $\boldsymbol{u}$ and $\boldsymbol{v}$ vector valued, and S tensor valued. Then*

1. $D_\Gamma(\Phi \boldsymbol{u}) = \boldsymbol{u} \otimes \nabla_\Gamma \Phi + \Phi D_\Gamma \boldsymbol{u}$,
2. $div_\Gamma(\Phi \boldsymbol{u}) = \Phi div_\Gamma \boldsymbol{u} + \boldsymbol{u} \cdot \nabla_\Gamma \Phi$,
3. $\nabla_\Gamma(\boldsymbol{u} \cdot \boldsymbol{v}) = D_\Gamma \boldsymbol{u}^T \boldsymbol{v} + D_\Gamma \boldsymbol{v}^T \boldsymbol{u}$,
4. $div_\Gamma(\boldsymbol{u} \otimes \boldsymbol{v}) = \boldsymbol{u} div_\Gamma \boldsymbol{v} + D_\Gamma \boldsymbol{u} \boldsymbol{v}$,
5. $div_\Gamma(S^T \boldsymbol{u}) = S \cdot D_\Gamma \boldsymbol{u} + \boldsymbol{u} \cdot div_\Gamma S$.

Lemma A.2 *(Divergence theorem). (See [12].) If $\boldsymbol{u} \in \mathcal{C}^1(\Gamma, \mathbb{R}^3)$, then*

$$\int_\Gamma div_\Gamma \boldsymbol{u} = \int_{\partial\Gamma} \boldsymbol{u} \cdot \boldsymbol{n}_s + \int_\Gamma H \boldsymbol{u} \cdot \boldsymbol{n},$$

where $\boldsymbol{n}_s$ is normal to $\partial\Gamma$, H is the mean curvature and $\boldsymbol{n}$ is a unit normal vector field on Γ.

In order to obtain first and second variation of the area operator for surfaces we need to compute some auxiliary derivatives. Recall that given V and W two finite-dimensional normed vector spaces, $\mathcal{D}$ an open subspace of V, and $f : \mathcal{D} \to W$, we say that f is differentiable at $x \in \mathcal{D}$ if there exists a linear transformation $Df(x) : V \to W$ such that

$$f(x+u) - f(x) = Df(x)[u] + o(u), \tag{16}$$

for any $u \in V$ with $x+u \in \mathcal{D}$, where $\|o(u)\|_W / \|u\|_V \to 0$ when $\|u\|_V \to 0$. We call $Df(x)$ the derivative of g at x.

Let $\mathcal{M}_{m\times n}$ be the space of m by n matrices and $\mathcal{M}_n = \mathcal{M}_{n\times n}$. It is possible to show (see [18]) that

1. If $T : V \to W$ is a linear transformation then $DT(u)[v] = T(v)$, for all $u, v \in V$.
2. If $f : \mathcal{M}_{m\times n} \to \mathcal{M}_n$ is given by $f(A) = A^T A$ then
$$Df(A)[B] = A^T B + B^T A, \qquad \text{for all } A, B \in \mathcal{M}_{m\times n}. \tag{17}$$
3. If $A \in \mathcal{M}_n$, then
$$D\det(A)[U] = \operatorname{tr}(\operatorname{cof}(A)^T U) = \det(A)\operatorname{tr}(A^{-1}U), \quad \text{for all } U \in \mathcal{M}_n, \tag{18}$$
with the last equality only valid if A is invertible.
4. If $\Phi(A) = A^{-1}$ for $A \in \mathcal{M}_n$ invertible then
$$D\Phi(A)[M] = -A^{-1}MA^{-1}, \qquad \text{for all } M \in \mathcal{M}_n. \tag{19}$$

We now state and prove some auxiliary variational derivatives of geometric objects.

Lemma A.3 *(First variation of $\sqrt{g}$). Let $g : \mathcal{R}^m(\Omega) \to C^{m-1}(\Omega;\mathbb{R})$ be given by $g(X) = \det(DX^T DX)$. Then, the variation of $\sqrt{g}$ is*

$$\left(\sqrt{g}\right)'(X)[\boldsymbol{U}] = div_\Gamma \boldsymbol{u} \circ X \sqrt{g}$$

for any $\boldsymbol{U} \in \boldsymbol{\mathcal{V}}$, where $\boldsymbol{u} = \boldsymbol{U} \circ X^{-1}$ is the push-forward of $\boldsymbol{U}$.

Proof. To obtain $(\sqrt{g})'(X)[\boldsymbol{U}]$, where $g(X) = \det G(X)$ and $G(X) = DX^T DX$, we use the chain rule and formulas as follows: (18) and (19). Then, we have

$$(\sqrt{g})'(X)[\boldsymbol{U}] = \frac{1}{2\sqrt{g}}(\det G)'(X)[\boldsymbol{U}] = \frac{1}{2\sqrt{g}}\det G \ \operatorname{tr}(G^{-1}G'(X)[\boldsymbol{U}])$$

Now, recall that $S \cdot P = \operatorname{tr}(S^T P)$, so that

$$\begin{aligned}(\sqrt{g})'(X)[\boldsymbol{U}] &= \frac{\sqrt{g}}{2} G^{-1} \cdot (DX^T D\boldsymbol{U} + D\boldsymbol{U}^T DX) \\ &= \sqrt{g}\, G^{-1} \cdot DX^T D\boldsymbol{U} = \sqrt{g} DX G^{-1} \cdot DU,\end{aligned}$$

where in the last we have used that $S \cdot P = S \cdot P^T$, if S is a symmetric tensor. Then

$$G^{-1} \cdot DX^T D\boldsymbol{U} = \operatorname{tr}(D\boldsymbol{U} G^{-1} DX^T) = div_\Gamma \boldsymbol{u} \circ X. \qquad \square$$

Lemma A.4 *(First variation of the normal). Let $X \in \mathcal{R}^m(\Omega)$, if $\boldsymbol{N} \in \mathcal{C}^1(\Omega, \mathbb{R}^3)$ is such that the push-forward $\boldsymbol{n} = \boldsymbol{N} \circ X^{-1}$ is the unit normal vector field of the surface $\Gamma = X(\Omega)$, then*

$$\boldsymbol{N}'(X)[\boldsymbol{U}] = -D_\Gamma \boldsymbol{u}^T \boldsymbol{n} = -\nabla_\Gamma(\boldsymbol{u} \cdot \boldsymbol{n}) + D_\Gamma \boldsymbol{n}\, \Pi\, \boldsymbol{u},$$

for any $\boldsymbol{U} \in \boldsymbol{\mathcal{V}}$, where the right-hand side is evaluated in $P \in \Omega$ and the left one in $p = X(P) \in \Gamma$.

Proof. Since $\boldsymbol{N} \cdot \boldsymbol{N} \equiv 1$, we have $\boldsymbol{N}'(X)[\boldsymbol{U}] \cdot \boldsymbol{N} = 0$, for any $\boldsymbol{U} \in \boldsymbol{\mathcal{V}}$. Then $\boldsymbol{N}'(X)[\boldsymbol{U}] \in T_p(\Gamma)$ and we can write $\boldsymbol{N}'(X)[\boldsymbol{U}] = DX\boldsymbol{A}$, for some $\boldsymbol{A} \in \mathbb{R}^2$. If we denote with $\{\boldsymbol{e}_1, \boldsymbol{e}_2\}$ the canonical basis of $\mathbb{R}^2$, then $DX\boldsymbol{e_i} \cdot \boldsymbol{N} \equiv 0$ and this implies

$$\boldsymbol{N}'(X)[\boldsymbol{U}] \cdot DX\boldsymbol{e}_i = -(DX)'[\boldsymbol{U}]\boldsymbol{e}_i \cdot \boldsymbol{N} = -D\boldsymbol{U}\boldsymbol{e_i} \cdot \boldsymbol{N}$$

and also

$$DX^T DX\boldsymbol{A} \cdot \boldsymbol{e_i} = -D\boldsymbol{U}^T \boldsymbol{N} \cdot \boldsymbol{e_i}, \qquad \text{for } i = 1, 2.$$

Since $G = DX^T DX$ is invertible, $\boldsymbol{A} = -G^{-1} D\boldsymbol{U}^T \boldsymbol{N}$ and then $\boldsymbol{N}'(X)[\boldsymbol{U}] = -(D\boldsymbol{U} G^{-1} DX^T)^T \boldsymbol{N}$. Since $D\boldsymbol{U} G^{-1} DX^T$ is the matrix representation in canonical basis of $D_\Gamma \boldsymbol{u}$, we obtain the first identity.

To prove that

$$D_\Gamma \boldsymbol{u}^T \boldsymbol{n} = \nabla_\Gamma(\boldsymbol{u}\cdot\boldsymbol{n}) - D_\Gamma \boldsymbol{n}\,\Pi\,\boldsymbol{u},$$

we split $\boldsymbol{u}$ into its normal and tangential parts: $\boldsymbol{u} = \boldsymbol{u}_n + \boldsymbol{u}_t$, where $\boldsymbol{u}_n = (\boldsymbol{u}\cdot\boldsymbol{n})\boldsymbol{n}$ and $\boldsymbol{u}_t = \Pi\boldsymbol{u}$. Applying Lemma A.1 we have $D_\Gamma \boldsymbol{u}_n = \boldsymbol{n}\otimes\nabla_\Gamma(\boldsymbol{u}\cdot\boldsymbol{n}) + (\boldsymbol{u}\cdot\boldsymbol{n})D_\Gamma\boldsymbol{n}\Pi$. Then $D_\Gamma \boldsymbol{u}_n^T\boldsymbol{n} = \nabla_\Gamma(\boldsymbol{u}\cdot\boldsymbol{n})$.

Finally, if we derive $\boldsymbol{u}_t\cdot\boldsymbol{n}\equiv 0$ we obtain

$$D_\Gamma \boldsymbol{u}_t^T\boldsymbol{n} = -D_\Gamma\boldsymbol{n}^T\boldsymbol{u}_t = -D_\Gamma\boldsymbol{n}\,\Pi\,\boldsymbol{u},$$

where we have used that $D_\Gamma\boldsymbol{n}$ is symmetric in $T_p(\Gamma)$. □

A.2. Proof of Lemma 3.1

Starting from (1) and using Lemma A.3 we get

$$J'(X)[\boldsymbol{U}] = \left(\int_\Omega \sqrt{g}\,dP\right)'(X)[\boldsymbol{U}] = \int_\Omega (\sqrt{g})'(X)[\boldsymbol{U}]\,dP = \int_\Gamma div_\Gamma \boldsymbol{u}\,dp, \tag{20}$$

where we have use that $dp = \sqrt{g}\,dP$. Finally, using divergence theorem (Lemma A.2) and that $\boldsymbol{u} = 0$ in $\partial\Gamma$, we obtain the desired result. □

A.3. Proof of Lemma 4.1

We first prove a formula for the second variation of the area functional.

Lemma A.5 *(Second variation of J). If $X\in\mathcal{R}^m(\Omega)$ and $\Gamma = X(\Omega)$, we have*

$$J''(X)[\boldsymbol{U}][\boldsymbol{V}] = \int_\Gamma D_\Gamma\boldsymbol{u}^T\boldsymbol{n}\cdot D_\Gamma\boldsymbol{v}^T\boldsymbol{n} + div_\Gamma\boldsymbol{u}\,div_\Gamma\boldsymbol{v} - D_\Gamma\boldsymbol{u}\,\Pi\cdot D_\Gamma\boldsymbol{v}^T, \tag{21}$$

for any $\boldsymbol{U},\boldsymbol{V}\in\boldsymbol{\mathcal{V}}$.

Proof. Using (20), we obtain the following expression of $J'(X)$ in terms of reference space Ω: $J'(X)[\boldsymbol{U}] = \int_\Omega DXG^{-1}\cdot D\boldsymbol{U}\sqrt{g}$. For a fixed $\boldsymbol{U}\in\boldsymbol{\mathcal{V}}$ define $L(X) := J'(X)[\boldsymbol{U}]$ and let us compute its first variation. Let $\boldsymbol{V}\in\boldsymbol{\mathcal{V}}$, by the product rule we have

$$\begin{aligned} L'(X) &= \int_\Omega (DX\sqrt{g}G^{-1})'[\boldsymbol{V}]\cdot D\boldsymbol{U} \\ &= \underbrace{\int_\Omega DX(\sqrt{g}G^{-1})'[\boldsymbol{V}]\cdot D\boldsymbol{U}}_{A} + \underbrace{\int_\Omega D\boldsymbol{V}G^{-1}\cdot D\boldsymbol{U}\sqrt{g}}_{B}. \end{aligned}$$

For the first term A, we use the product rule one more time obtaining

$$A = \underbrace{\int_\Omega (\sqrt{g})'[\boldsymbol{V}]\left(DXG^{-1}\cdot D\boldsymbol{U}\right)}_{A_1} + \underbrace{\int_\Omega DX(G^{-1})'[\boldsymbol{V}]\cdot D\boldsymbol{U}\sqrt{g}}_{A_2}.$$

Using the expression for $(\sqrt{g})'[\boldsymbol{V}]$ from (20),

$$\begin{aligned} A_1 &= \int_\Omega \left(DXG^{-1}\cdot D\boldsymbol{V}\right)\left(DXG^{-1}\cdot D\boldsymbol{U}\right)\sqrt{g} \\ &= \int_\Omega \operatorname{tr}\left(D\boldsymbol{V}G^{-1}DX^T\right)\operatorname{tr}\left(D\boldsymbol{U}G^{-1}DX^T\right)\sqrt{g} \\ &= \int_\Gamma div_\Gamma\boldsymbol{v}\,div_\Gamma\boldsymbol{u}. \end{aligned} \tag{22}$$

Besides, by (19) we have $(G^{-1})'[\boldsymbol{V}] = -G^{-1}G'[\boldsymbol{V}]G^{-1}$, and by (17), $G'[\boldsymbol{V}] = DX^T D\boldsymbol{V} + D\boldsymbol{V}^T DX$. Then

$$\begin{aligned} A_2 &= -\int_\Omega \left(DXG^{-1}DX^T D\boldsymbol{V} G^{-1} + DXG^{-1}D\boldsymbol{V}^T DXG^{-1} \right) \cdot D\boldsymbol{U}\sqrt{g} \\ &= A_{21} + A_{22}. \end{aligned}$$

Observe that

$$\begin{aligned} A_{21} + B &= \int_\Omega \left(I - DXG^{-1}DX \right) D\boldsymbol{V} G^{-1} \cdot D\boldsymbol{U}\sqrt{g} \\ &= \int_\Omega \left(I - DXG^{-1}DX \right) D\boldsymbol{V} G^{-1} DX^T \cdot D\boldsymbol{U} G^{-1} DX^T \sqrt{g}, \end{aligned}$$

and by (6), we have that $I - DXG^{-1}DX = \boldsymbol{n} \otimes \boldsymbol{n} \circ X$. Hence

$$A_{21} + B = \int_\Gamma (\boldsymbol{n} \otimes \boldsymbol{n})\, D_\Gamma \boldsymbol{v} \cdot D_\Gamma \boldsymbol{u} = \int_\Gamma D_\Gamma \boldsymbol{v}^T \boldsymbol{n} \cdot D_\Gamma \boldsymbol{v}^T \boldsymbol{n}, \tag{23}$$

where we have used tensor product properties.

Finally, we write A_{22} as an integral over Γ:

$$A_{22} = -\int_\Gamma (D_\Gamma \boldsymbol{v}\, \Pi)^T \cdot D_\Gamma \boldsymbol{u}\, \Pi = -\int_\Gamma D_\Gamma \boldsymbol{v}^T \cdot D_\Gamma \boldsymbol{u}\, \Pi, \tag{24}$$

where we use that $\Pi^T = \Pi^2 = \Pi$.

Using that $J''(X)[\boldsymbol{V}][\boldsymbol{U}] = (A_{21} + B) + A_1 + A_{22}$, the assertion follows from (22), (23) and (24). □

Proof of Lemma 4.1. First note that $F(X)[\boldsymbol{U}] = J'(X)[\boldsymbol{U}] - C\int_\Gamma \boldsymbol{n} \cdot \boldsymbol{u}$. Since we already have an expression for $J''(X)[\boldsymbol{U}][\boldsymbol{V}]$, we only have to prove that

$$\left(\int_\Gamma \boldsymbol{n} \cdot \boldsymbol{u} \right)' (X)[\boldsymbol{U}] = \int_\Gamma (\boldsymbol{u} \cdot \boldsymbol{n}) div_\Gamma \boldsymbol{v} - D_\Gamma \boldsymbol{v}^T \boldsymbol{n} \cdot \boldsymbol{u}.$$

Observe that

$$\begin{aligned} \left(\int_\Gamma \boldsymbol{n} \cdot \boldsymbol{u} \right)' (X)[\boldsymbol{V}] &= \int_\Omega \left(\boldsymbol{N}\sqrt{g} \right)' (X)[\boldsymbol{V}] \cdot \boldsymbol{U} \\ &= \int_\Omega \boldsymbol{N}'(X)[\boldsymbol{V}]\sqrt{g} \cdot \boldsymbol{U} + \boldsymbol{N}(\sqrt{g})'(X)[\boldsymbol{V}] \cdot \boldsymbol{U} \\ &= \int_\Gamma D_\Gamma \boldsymbol{v}^T \boldsymbol{n} \cdot \boldsymbol{u} + (\boldsymbol{n} \cdot \boldsymbol{u}) div_\Gamma \boldsymbol{v}, \end{aligned}$$

where in the last step we have used Lemmas A.4 and A.3. □

A.4. Proof of Proposition 4.2

Let us consider the identity (10) with $\boldsymbol{U} = \Phi\boldsymbol{N}$ and $\boldsymbol{V} = \Psi\boldsymbol{N}$, where Φ and Ψ belong to $\mathcal{V} = \{\phi \in \mathcal{C}^m(\Omega, \mathbb{R}) : \phi|_{\partial\Omega} = 0\}$. We want to show that

$$F'(X)[\Phi\boldsymbol{N}][\Psi\boldsymbol{N}] = \int_\Gamma \nabla_\Gamma \phi \cdot \nabla_\Gamma \psi + \int_\Gamma (2K - CH)\phi\psi, \tag{25}$$

where K and H are the Gaussian and the mean curvature of $\Gamma = X(\Omega)$, respectively, and C is the prescribed constant mean curvature. Here, as usual, the push-forward of Φ and Ψ is given by $\phi = \Phi \circ X^{-1}$ and $\psi = \Psi \circ X^{-1}$, respectively, so that $\boldsymbol{u} = \phi\boldsymbol{n}$ and $\boldsymbol{v} = \psi\boldsymbol{n}$. Note that, by Lemma A.1, $D_\Gamma \boldsymbol{u} = D_\Gamma(\phi\boldsymbol{n}) = \phi D_\Gamma \boldsymbol{n}\, \Pi + \boldsymbol{n} \otimes \nabla_\Gamma \phi$. This implies $D_\Gamma \boldsymbol{u}^T \boldsymbol{n} = \nabla_\Gamma \phi$ and $div_\Gamma \boldsymbol{u} = \phi\, \mathrm{tr}(D_\Gamma \boldsymbol{n}) = \phi H$. Also, using some properties of the product $S \cdot Q = \mathrm{tr}(S^T Q)$, we obtain

$$
\begin{aligned}
(D_\Gamma \boldsymbol{u}\,\Pi)^T \cdot D_\Gamma \boldsymbol{v}\,\Pi &= (\nabla_\Gamma \phi \otimes \boldsymbol{n} + \phi D_\Gamma \boldsymbol{n}\Pi)^T \cdot (\nabla_\Gamma \psi \otimes \boldsymbol{n} + \psi D_\Gamma \boldsymbol{n}\Pi) \\
&= \phi\,\psi\,(D_\Gamma \boldsymbol{n}^T \cdot D_\Gamma \boldsymbol{n}) \\
&= \phi\,\psi\ \mathrm{tr}(D_\Gamma \boldsymbol{n}^2).
\end{aligned}
$$

Then

$$
\begin{aligned}
&D_\Gamma \boldsymbol{u}^T \boldsymbol{n} \cdot D_\Gamma \boldsymbol{v}^T \boldsymbol{n} + div_\Gamma \boldsymbol{u}\, div_\Gamma \boldsymbol{v} - D_\Gamma \boldsymbol{u}\,\Pi \cdot D_\Gamma \boldsymbol{v}^T \\
&\qquad = \nabla_\Gamma \phi \cdot \nabla_\Gamma \psi + \phi\,\psi\ \mathrm{tr}(D_\Gamma \boldsymbol{n})^2 - \phi\,\psi\ \mathrm{tr}(D_\Gamma \boldsymbol{n}^2) \\
&\qquad = \nabla_\Gamma \phi \cdot \nabla_\Gamma \psi + \phi\,\psi 2K,
\end{aligned} \tag{26}
$$

since the Gaussian curvature $K = \kappa_1\kappa_2 = \frac{1}{2}\left[(tr D_\Gamma \boldsymbol{n})^2 - tr(D_\Gamma \boldsymbol{n}^2)\right]$.

Finally, since

$$
C\left(\boldsymbol{u} \cdot D_\Gamma \boldsymbol{v}^T \boldsymbol{n} - (\boldsymbol{u} \cdot \boldsymbol{n}) div_\Gamma \boldsymbol{v}\right) = C\,(0 - \phi\,\psi\ \mathrm{tr}(D_\Gamma \boldsymbol{n})) = -\phi\psi HC, \tag{27}
$$

we add (26) and (27) and integrate over Γ to obtain the desired result (25). □

A.5. Example of non-invertibility of $F'(X)[\boldsymbol{U}][\boldsymbol{V}]$

Now we provide an example showing the lack of invertibility of $F'(X)[\boldsymbol{U}][\boldsymbol{V}]$ if arbitrary directions for perturbations are allowed. We consider the simplest case of minimal surfaces, i.e., the prescribed mean curvature is $C = 0$ and thus $F = J'$.

Proposition A.6. *There exists a (non-trivial) regular surface $\Gamma = X(\Omega)$ and a non-trivial function $\boldsymbol{U} \in \boldsymbol{\mathcal{V}}$ such that*

$$
F'(X)[\boldsymbol{U}][\boldsymbol{V}] = 0, \quad \forall V \in \boldsymbol{\mathcal{V}}.
$$

Proof. Let Ω be an open subset of $\mathbb{R}^2$ and let $X \in \mathcal{R}^m(\Omega)$ be a parametrization of a regular surface $\Gamma = X(\Omega)$ such that $\Gamma_0 := X(\Omega_0)$ is planar, for some nonempty open set $\Omega_0 \subset \Omega$. Let $\Phi \in C_0^\infty(\Omega_0)$ with $\Phi \not\equiv 0$, and let $\phi = \Phi \circ X^{-1}$ so that $\boldsymbol{u} = \nabla_\Gamma \phi \in \boldsymbol{\mathcal{V}}$ is tangential to Γ and $\boldsymbol{u} = \boldsymbol{0}$ in $\Gamma \setminus \Gamma_0$, and let $V \in \boldsymbol{\mathcal{V}}$ be arbitrary. Then, from (10) we have,

$$
F'(X)[\boldsymbol{U}][\boldsymbol{V}] = \int_{\Gamma_0} D_\Gamma \boldsymbol{u}^T \boldsymbol{n} \cdot D_\Gamma \boldsymbol{v}^T \boldsymbol{n} + \int_{\Gamma_0} div_\Gamma \boldsymbol{u}\, div_\Gamma \boldsymbol{v} - D_\Gamma \boldsymbol{u}\,\Pi \cdot \Pi\, D_\Gamma \boldsymbol{v}^T \tag{28}
$$

By reparametrization we may assume, without loss of generality, that $X(\Omega_0) = \Omega_0$ and moreover, $X\begin{pmatrix} w \\ z \end{pmatrix} = \begin{pmatrix} w \\ z \\ 0 \end{pmatrix}$ for all $\begin{pmatrix} w \\ z \end{pmatrix} \in \Omega_0$. Hence, in $\Omega_0 = \Gamma_0$,

$$
DX = \begin{bmatrix} 1 & 0 \\ 0 & 1 \\ 0 & 0 \end{bmatrix}, \qquad \boldsymbol{U}\begin{pmatrix} w \\ z \end{pmatrix} = \begin{bmatrix} U^1\begin{pmatrix} w \\ z \end{pmatrix} \\ U^2\begin{pmatrix} w \\ z \end{pmatrix} \\ 0 \end{bmatrix}, \qquad D\boldsymbol{U}\begin{pmatrix} w \\ z \end{pmatrix} = \begin{bmatrix} U^1_w\begin{pmatrix} w \\ z \end{pmatrix} & U^1_z\begin{pmatrix} w \\ z \end{pmatrix} \\ U^2_x\begin{pmatrix} w \\ z \end{pmatrix} & U^2_z\begin{pmatrix} w \\ z \end{pmatrix} \\ 0 & 0 \end{bmatrix}.
$$

Then the entries in the third row and in the third column of $D\boldsymbol{U}G^{-1}DX^T$ are all zero, whence $D_\Gamma \boldsymbol{u}^T \boldsymbol{n} = D_\Gamma \boldsymbol{u}^T \begin{pmatrix} 0 \\ 0 \\ 1 \end{pmatrix} = \boldsymbol{0}$. The first integral in (28) is thus zero.

Observe now that $div_\Gamma \boldsymbol{u} = U^1_w + U^2_z$ and $D_\Gamma \boldsymbol{u}^T \cdot D_\Gamma \boldsymbol{v} = U^1_w V^1_w + U^2_z V^2_z + U^1_z V^2_w + U^2_w V^1_z$. Then

$$
\int_{\Gamma_0} div_\Gamma \boldsymbol{u} div_\Gamma \boldsymbol{v} - D_\Gamma \boldsymbol{u}^T \cdot D_\Gamma \boldsymbol{v} = \int_\Omega U^1_w V^2_z - U^1_z V^2_w + \int_\Omega U^2_z V^1_w - U^2_w V^1_z.
$$

Since $\boldsymbol{U}$ and $\boldsymbol{V}$ are $\mathcal{C}^2$ and vanish on $\partial\Omega$, the two integrals on the right are zero, due to integration by parts, and thus we have found $\boldsymbol{U}$ such that $F'(X)[\boldsymbol{U}][\boldsymbol{V}] = 0$ for all $\boldsymbol{V} \in \boldsymbol{\mathcal{V}}$. □

References

[1] J. Plateau, Statique Expérimentale et Théoretique des Liquides Soumis aux Seules Forces Moléculaires, vol. 2, Gauthiers-Villars, 1873.

[2] C.V. Boys, et al., Soap-Bubbles, and the Forces Which Mould Them, Cornell University Library, 1890.

[3] U. Dierkes, S. Hildebrandt, F. Sauvigny, Minimal Surfaces, 2nd ed., Grundlehren der Mathematischen Wissenschaften (Fundamental Principles of Mathematical Sciences), vol. 339, Springer, Heidelberg, 2010. With assistance and contributions by A. Küster and R. Jakob.

[4] J.C.C. Nitsche, Lectures on Minimal Surfaces, vol. 1, Introduction, Fundamentals, Geometry and Basic Boundary Value Problems, Cambridge University Press, Cambridge, 1989. Translated from German by Jerry M. Feinberg, with a German foreword.

[5] J. Metzger, Numerical computation of constant mean curvature surfaces using finite elements, Class. Quantum Gravity 21 (19) (2004) 4625–4646, http://dx.doi.org/10.1088/0264-9381/21/19/010.
[6] G. Dziuk, J.E. Hutchinson, Finite element approximations to surfaces of prescribed variable mean curvature, Numer. Math. 102 (4) (2006) 611–648, http://dx.doi.org/10.1007/s00211-005-0649-7.
[7] T.J.R. Hughes, J.A. Cottrell, Y. Bazilevs, Isogeometric analysis: CAD, finite elements, NURBS, exact geometry and mesh refinement, Comput. Methods Appl. Mech. Eng. 194 (39–41) (2005) 4135–4195, http://dx.doi.org/10.1016/j.cma.2004.10.008.
[8] M.S. Pauletti, M. Martinelli, N. Cavallini, P. Antolin, igatools: an isogeometric analysis library, SIAM J. Sci. Comput. 37 (4) (2015) C465–C496.
[9] G. Dziuk, J.E. Hutchinson, The discrete Plateau problem: convergence results, Math. Comput. 68 (226) (1999) 519–546, http://dx.doi.org/10.1090/S0025-5718-99-01026-1.
[10] Ø. Tråsdahl, E.M. Rønquist, High order numerical approximation of minimal surfaces, J. Comput. Phys. 230 (12) (2011) 4795–4810, http://dx.doi.org/10.1016/j.jcp.2011.03.003.
[11] T.J. Willmore, Riemannian Geometry, Oxford Science Publications, The Clarendon Press, Oxford University Press, New York, 1993.
[12] M. Delfour, J. Zolesio, Shapes and Geometries, 2nd ed., Society for Industrial and Applied Mathematics, 2011.
[13] L.A. Piegl, W. Tiller, The NURBs Book, Monographs in Visual Communication, Springer-Verlag GmbH, 1997.
[14] A. Laurain, S.W. Walker, Droplet footprint control, SIAM J. Control Optim. 53 (2) (2015) 771–799, http://dx.doi.org/10.1137/140979721.
[15] J.-F. Gerbeau, T. Leliévre, Generalized Navier boundary condition and geometric conservation law for surface tension, Comput. Methods Appl. Mech. Eng. 198 (5–8) (2009) 644–656, http://dx.doi.org/10.1016/j.cma.2008.09.011.
[16] J. Haslinger, R. Mäkinen, Introduction to Shape Optimization, Society for Industrial and Applied Mathematics, 2003.
[17] S. Walker, The Shapes of Things, Society for Industrial and Applied Mathematics, Philadelphia, 2015.
[18] M.E. Gurtin, An Introduction to Continuum Mechanics, Mathematics in Science and Engineering, vol. 158, Academic Press, Inc. [Harcourt Brace Jovanovich, Publishers], New York, London, 1981.